# ASSESSMENT OF COMPUTATIONAL TECHNIQUES FOR THE PREDICTION OF ACOUSTIC SOURCES FROM LIFTING SURFACES USING LES AND DNS

**Tom A. Smith*** **and Yiannis Ventikos***

* University College London, Dept. Mechanical Engineering, London, WC1E 7JE, United Kingdom
e-mail: **tom.smith.17@ucl.ac.uk**

**Key words:** DNS, LES, Boundary Layer Transition, Trailing Edge Flow

**Abstract.** The acoustic field produced by the flow over a lifting surface is closely linked to the dynamics of the boundary layer. The location and mechanism of the transition strongly influences the character of the trailing edge flow and surface pressure fluctuations and so accurately predicting the transition process is critical for acoustic analyses. In this study, a comparison of DNS and LES is undertaken for a transitional boundary layer flow over a foil at a moderate Reynolds number. The effects of the of sub-filter scale model, discretisation scheme and mesh resolution are considered to better understand how LES can be used to accurately resolve external boundary layer and trailing edge flows. Significant differences are seen for the different modelling approaches and the reasons for this are explored. A second case is then considered using LES which has a very different boundary layer and trailing edge flow. This case highlights the important link between the transitional boundary layer dynamics, trailing edge flow and the acoustic field.

## 1 INTRODUCTION

Transitional boundary layers represent an important class of flows in marine engineering. For flows over lifting surfaces at moderate to high Reynolds numbers such as propeller, hydrofoil and pump flows, the boundary layer dynamics have a significant influence on the trailing edge flow and resulting noise. It has been shown experimentally, for example [1], that large amplitude tonal noise can be generated at a foil trailing edge if the pressure-side boundary layer is still transitional at the trailing edge. This occurs if the Tollmien-Schlichting (T-S) instabilities responsible for the transition become amplified by a separated region at the trailing edge. If the transition occurs closer to the leading edge, the 2D structures associated with the Tollmien-Schlichting instabilities will have broken down into 3D structures that will scatter as broadband noise at the trailing edge. Accurately capturing the location and mechanism of the transition is therefore paramount for acoustic analyses.

Whilst DNS has provided detailed insights into the flow physics of transitional boundary layers, for example in [2], [3], this method is still far too expensive to apply to many practical flows of interest in hydro-acoustics. Therefore, attention over the past decade has turned to the use of large eddy simulations for acoustic analyses, which allow for the larger turbulent scales to be resolved whilst modelling the smaller scales. A number of recent studies into trailing edge noise, e.g. [4], [5] have used large eddy simulations to provide the source terms for acoustic models such as those developed by Curle, [6] and Ffowcs-Williams and Hawkings, [7]. Most such studies provide only limited verification and uncertainty analysis, and grid sensitivity studies are far less common than for RANS-based analyses. A wide range of approaches are used in terms of sub-filter scale modelling and discretisation, with little published information on the sensitivity of the boundary layer dynamics to the different methods used. Experimental results such as [1], [8] have shown that small changes in the operating conditions can lead to large changes in the boundary layer and acoustic field. Therefore, in order to use LES as a predictive tool, a better understanding of how well different modelling techniques capture these dynamics is needed.

In this study, 2 separate cases are considered. For Case 1, both LES and DNS are used to model the flow over a NACA0012 foil at a Reynolds number of $Re = 10^5$ and an angle of attack of $\alpha = 4°$. Two sub-filter scale models are used and different approaches to the discretisation of the convective terms are considered. Grid independent DNS data are obtained which provide an excellent benchmark against which a number of large eddy simulations are compared. This provides a better understanding of how well different modelling approaches capture the transition process and resulting turbulent boundary layer. Case 2 then takes the best approaches from Case 1 and considers the flow with a Reynolds number of $Re = 1.5 \times 10^5$ and a 0° angle of attack. Unlike the broadband trailing edge flow and surface pressure field observed for Case 1, experiments in [8] have shown that the second case is dominated by narrowband fluctuations due to the presence of Tollmien-Schlichting waves close to the trailing edge. Thus by considering these cases we are able to explore the physical relationship between the boundary layer transition and the trailing edge flow as well as understand how LES can be used to analyse this important class of flows.

## 2 METHODS

The governing equations for an incompressible Newtonian fluid are given below.

$$\frac{\partial U_i}{\partial x_i} = 0 \tag{1}$$

$$\frac{\partial U_j}{\partial t} + U_i \frac{\partial U_j}{\partial x_i} = -\frac{1}{\rho}\frac{\partial p}{\partial x_j} + \nu \frac{\partial^2 U_j}{\partial x_i^2} \tag{2}$$

For Direct Numerical Simulation, all of the flow scales are resolved and so no further modelling is required. For large-eddy simulation, the flow field is split into a resolved part and a modelled part by spatially filtering the continuity and momentum equations. The latter part, representing the higher wave-number turbulence, is then modelled using a sub-filter scale model analogous

to the turbulence models used in a RANS approach. The filtered equations are derived by introducing a general filtering operator, G, to each variable:

$$\overline{\phi}(\mathbf{x},t) = \int_V G(\mathbf{r},\mathbf{x})\phi(\mathbf{x}-\mathbf{r},t)d\mathbf{r} \tag{3}$$

Applying the filter to each of the variables, the filtered equations are obtained:

$$\frac{\partial \bar{U}_j}{\partial t} + U_j\frac{\partial \bar{U}_i}{\partial x_i} = -\frac{1}{\rho}\frac{\partial \bar{p}}{\partial x_j} + \nu\frac{\partial^2 \bar{U}_j}{\partial x_i \partial x_i} - \frac{\partial \tau_{ij}}{\partial x_i} \tag{4}$$

where

$$\tau_{ij} = \overline{U_i U_j} - \bar{U}_i\bar{U}_j \tag{5}$$

The filtered equations given by equation 4 are not closed and so we must introduce an additional model to account for the effects of the sub-filter scale (SFS) stresses, $\tau_{ij}$. In this study, two different models for the sub-filter scale stresses are considered: the Smagorinsky model and the Local Dynamic k model. The Smagorinsky model, [9], is widely used and is an eddy viscosity model based on a characteristic length, which is usually defined by the grid size. It is also necessary, when using this model, to apply a damping function at walls to force the sub-filter scale viscosity to zero. To this end, a van Driest damping function, [10], is applied in this work. The second sub-filter scale model considered is the Localised Dynamic k Model developed by Kim and Menon, [11]. This is a one-equation transport model for the sub-filter scale turbulent kinetic energy. A dynamic procedure is used to determine the model coefficients which allows for the model to be tuned based only on the smaller resolved local flow scales.

The filter width is most commonly taken as the cube-root of the cell volume. However, this definition can result in the filter width being less than the stream-wise cell length for near-wall meshes, where anisotropic elements are used. This will introduce errors into the flow-field, as the smallest resolved scales will be under-resolved. To mitigate this problem, the following definition is therefore used:

$$\Delta = \lambda \cdot max(h_x, h_y, h_z), \quad \lambda \in \mathbb{N} \tag{6}$$

In this work, a value of $\lambda = 4$ is used which is based on the work in [12]. The coupled pressure/velocity fields are solved at each time step using the PISO algorithm with an algebraic multi-grid solver for the pressure correction equation. The time derivative is discretised using a 3-point backward scheme and a second-order central scheme is used for the spatial derivatives. The convective terms are also discretised using second-order schemes. For the direct numerical simulations, a pure central scheme is used exclusively whereas for the large eddy simulations, a range of blended approaches are considered which introduce a level of up-winding. The impact of this is discussed in the results.

The geometry considered is a NACA0012 foil with a chord length of 0.3m. For Case 1, a span of $s = 0.2c$ is used whereas a span of $s = 0.1c$ is used for Case 2. The foil has a trailing edge bluntness of $h_{TE} = 0.0025c$, which represents a sharp but physically realistic geometry. A block-structured mesh design is used with a C-grid around the foil. The mesh parameters are

| Case | Mesh | Turbulence | N cells ($\times 10^6$) | $\Delta x^+$ | $\Delta y^+$ | $\Delta z^+$ |
|---|---|---|---|---|---|---|
| 1 | A | LES | 1.8 | 42 | 38 | 0.6 |
| | B | LES | 4.1 | 29 | 23 | 0.6 |
| | C | LES | 8.7 | 16 | 15 | 0.6 |
| | D | DNS | 25 | 8 | 8 | 0.6 |
| | E | DNS | 58 | 6 | 5 | 0.4 |
| 2 | F | LES | 2.4 | 29 | 22 | 0.6 |
| | G | LES | 6.7 | 17 | 15 | 0.6 |

Table 1: Near wall mesh parameters for cases 1 and 2.

shown in table 1. Freestream boundary conditions are used at the inlet and outlet for both the pressure and velocity fields. The foil wall is treated as a no-slip boundary and the sub-filter scale turbulence quantities are set equal to zero on all boundaries apart from the outlet, where a zero-gradient condition is applied. Symmetry conditions are used for the side walls.

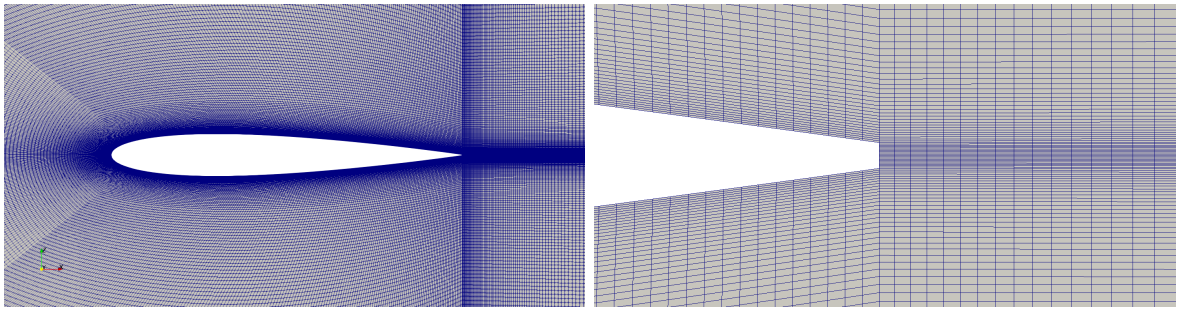

Figure 1: Design of mesh C showing the mesh around the foil and at the trailing edge

## 3 RESULTS AND DISCUSSION

### 3.1 Comparison of LES and DNS for Case 1

The DNS data for Case 1 show the growth of a separation bubble on the suction side prior to the transition of the boundary layer. The boundary layer re-attaches at around $x/c = 0.56$, after which a fully turbulent boundary layer forms. Results from meshes D and E are in excellent agreement, indicating grid independence of the results. A comparison of the suction-side boundary layer velocity profiles from the 2 meshes is shown in figure 2. Within the separation bubble, there is a region of reversed flow close to the wall which results in an unstable shear layer. Growing streamwise fluctuations are observed within this region which grow until the reattachment point. These fluctuations are dominated by a narrowband component centred around 140 Hz. After the boundary layer becomes fully turbulent, this component is lost and only broadband fluctuations are seen, as shown in figure 3. The turbulent boundary layer is then convected over the trailing edge, with the broadband turbulent structures decaying into the far

field. The pressure side of the foil remains laminar and attached all the way to the trailing edge.

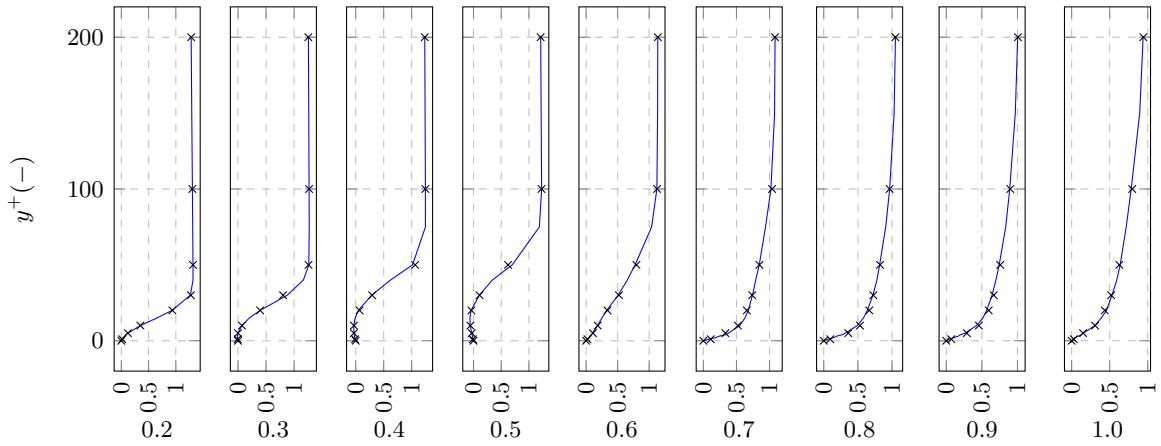


Figure 2: Mean streamwise velocity, $U_x/U_\infty$, in the boundary layer at different chord-wise locations. The solid line represents mesh E and the markers (x) represent mesh D.

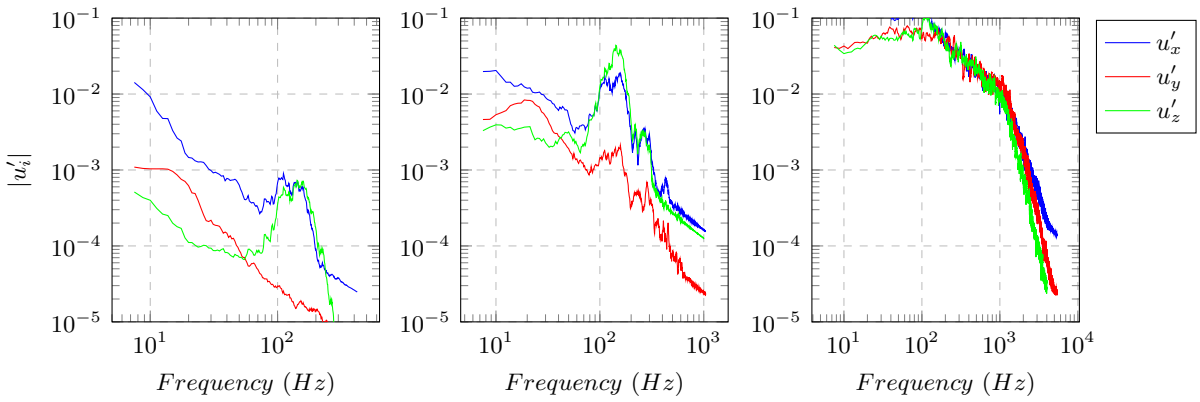


Figure 3: Spectral plots of the streamwise and spanwise velocity fluctuations from mesh E at $y^+ = 30$ for $x/c = 0.4,\ 0.5,\ 0.6$.

The large eddy simulations show very different results depending on the sub-filter scale modelling, discretisation scheme and mesh resolution. The interaction between these different components is complex and some of the key findings are explored here. Simulations conducted using the Smagorinsky model do not show any transition and so the boundary layer remains laminar on both the pressure and suction sides of the foil. This is irrespective of what discretisation scheme is used. For all three meshes, there is a separated region close to the trailing edge on the suction side which grows as the mesh is refined. Convergence towards the DNS data is not seen for these simulations. Instead, all exhibit trailing edge flows consistent with laminar boundary layers, with tonal fluctuations corresponding to von Kármán vortex shedding. This can be seen

in the velocity contour plots shown in figure 4. This behaviour contrasts sharply with that seen for the Dynamic k model, which does capture a transition in all cases.

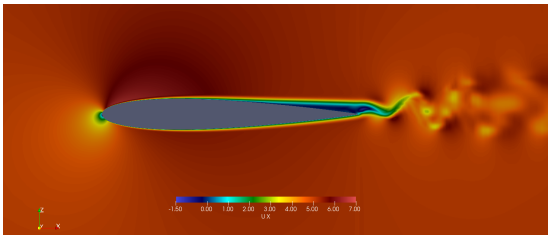

(a) Smagorinsky Model, Mesh C

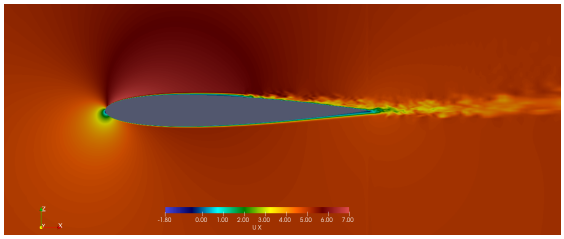

(b) Dynamic k Model, Mesh C

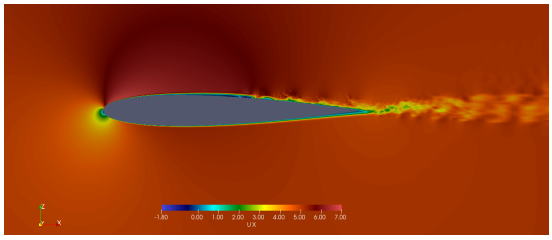

(c) DNS, Mesh D

Figure 4: Instantaneous streamwise velocity contours for $t = 20c/U$.

To explain the differences in the flow fields resolved by the two models, we consider the sub-filter scale viscosity in the boundary layer at $x/c = 0.4, 0.5, 0.6$, which covers the region over which the transition should occur. This is shown in figure 5. It can be seen that the dynamic k model is not active in the boundary layer for $x/c = 0.4$, with the sub-filter scale viscosity more than 2 orders of magnitude smaller than the molecular viscosity. The Smagorinsky model predicts a peak sub-filter scale viscosity of $6 \times 10^{-5}\ m^2 s^{-1}$, which is 4 times larger than the molecular viscosity. This prevents the growth of any disturbance in the boundary layer and so prevents the transition from occurring. The dynamic k model only becomes active at $x/c = 0.6$, which the DNS data show corresponds to the emergence of the smallest turbulent scales.

The effect of the differences in the SFS models on the prediction of the trailing edge noise can be seen by looking at the spectra of the trailing edge pressure fluctuations, shown in figure 6. The Smagorinsky model leads to a pressure spectrum dominated by tonal components at multiples of 65 Hz whereas a broadband spectrum is observed for the Dynamic k model, which is in agreements with the DNS data.

The errors associated with the discretisation scheme are small compared to the dissipative effects of the Smagorinsky model but become important when the Dynamic k model is used. For coarser meshes that use a pure central scheme, the flow field is dominated by unphysical velocity fluctuations caused by dispersion errors. These reduce as the mesh is refined, or as larger amounts of up-winding are introduced into the discretisation scheme. These errors can

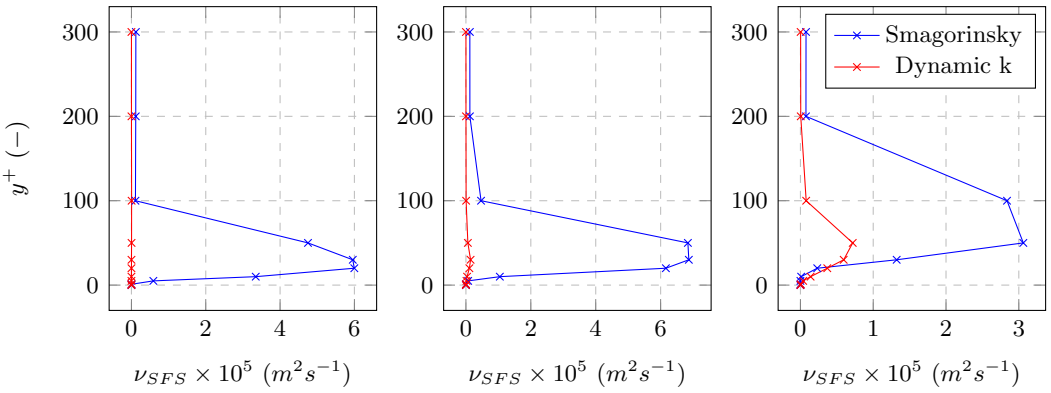


Figure 5: Comparison of the mean sub-filter scale viscosity in the boundary layer at $x/c = 0.4, 0.5, 0.6$ for the two SFS models. Results are for mesh C using a pure central scheme.

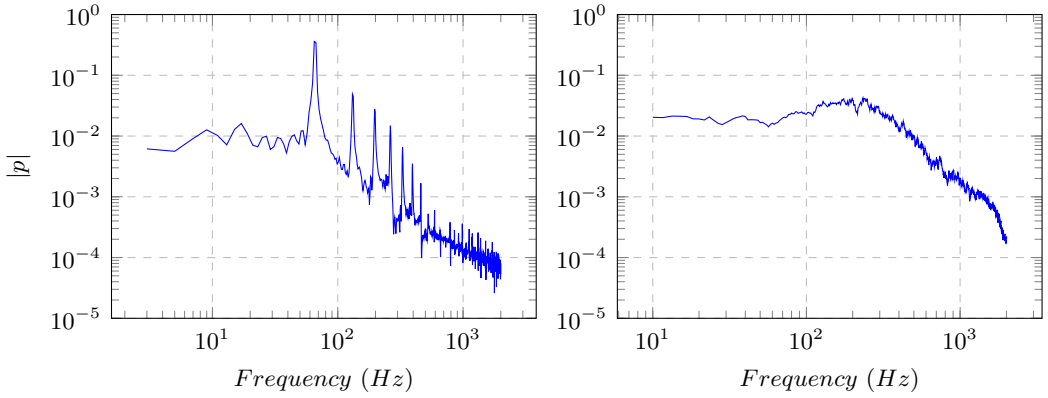


Figure 6: Trailing edge pressure spectra for (a) Smagorinsky model and (b) Dynamic k model. Results are taken from simulations using mesh C with a pure central scheme.

be visualised by looking at the vorticity in the flow field around the foil using the Q-criterion, as shown in Figure 7. It is also seen that coarser meshes, when combined with a pure central scheme fail to capture the separation bubble. Simulations using a blended scheme capture a separation bubble in all cases, with increasing agreement with the DNS data as the mesh is refined.

The effect of the dispersion errors on the boundary layer dynamics can be seen by looking at the change in the turbulent kinetic energy (TKE) in the boundary layer along the chord. This is shown for both the central scheme and a blended scheme with 25% upwinding in figures 8 and 9. While the DNS results show a sharp growth in the TKE between $x/c = 0.5$ and $x/c = 0.6$, the coarser meshes show a more gradual increase starting closer to the leading edge. This indicates that the transition is occurring earlier, and by a different mechanism. Analysis of the velocity fluctuations in the boundary layer reveal that the dispersion errors act in a similar way to free-stream turbulence and by-pass the natural transition of the boundary layer. This also explains

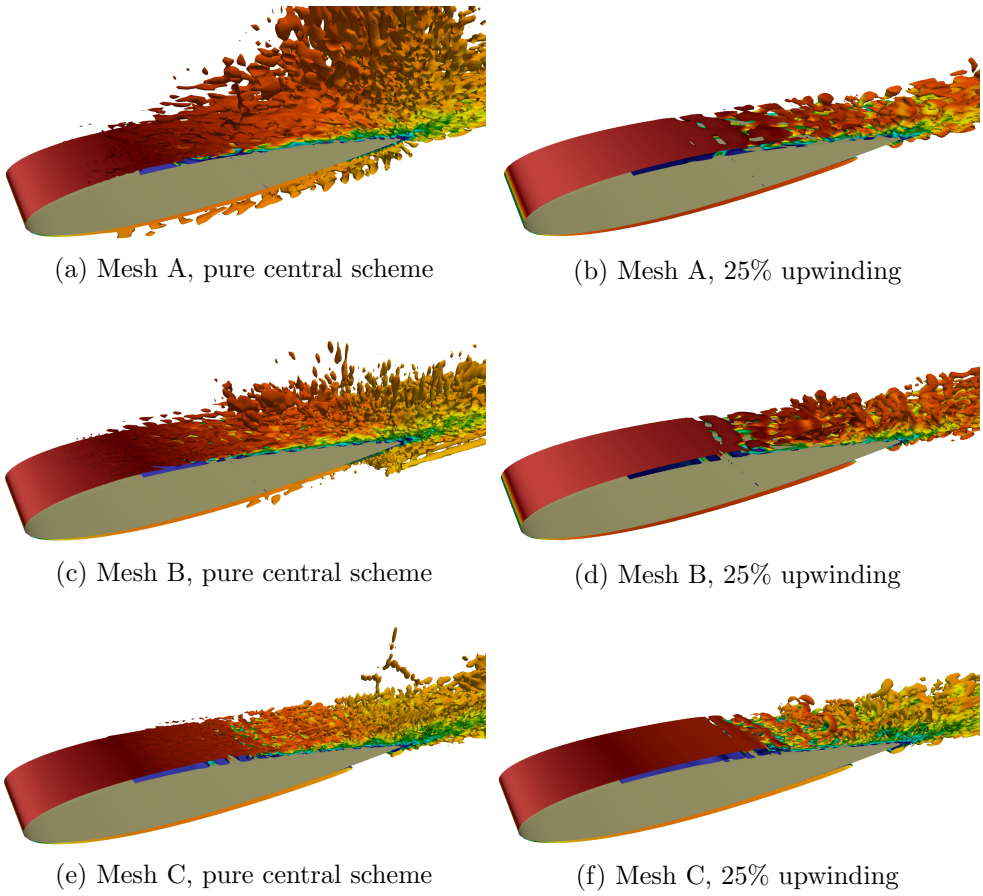

(a) Mesh A, pure central scheme

(b) Mesh A, 25% upwinding

(c) Mesh B, pure central scheme

(d) Mesh B, 25% upwinding

(e) Mesh C, pure central scheme

(f) Mesh C, 25% upwinding

Figure 7: Iso-contours of $Q = 100$ for different mesh resolutions and discretisation schemes. Contours coloured by velocity magnitude.

why no separation bubble is resolved in these cases, as the boundary layer is already turbulent.

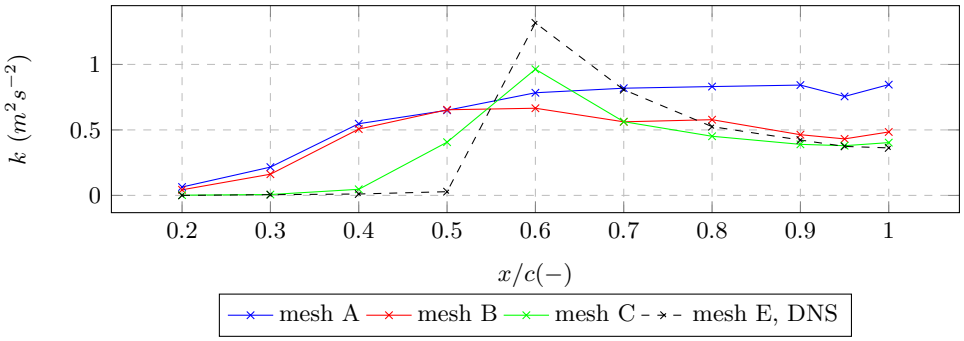


Figure 8: Resolved rms turbulent kinetic energy at $y^+ = 30$. DNS compared with LES with pure central differencing.

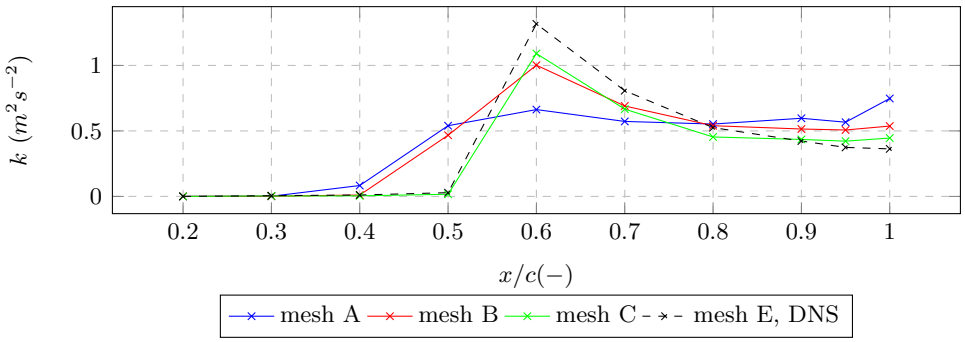


Figure 9: Resolved rms turbulent kinetic energy at $y^+ = 30$. DNS compared with LES with blended scheme using 25% upwinding.

The earlier transition leads to higher levels of turbulent kinetic energy at the trailing edge, particularly at lower frequencies. The effect of this is to increase the energy that is scattered as acoustic waves at the trailing edge. The dispersion errors will also create additional quadrupole noise sources if they are present in the acoustic source region. Spectral analysis of the erroneous fluctuations in the boundary layer reveals that they occur across a wide range of scales. As the dynamic SFS model is effective only in dissipating the smallest scales, the model does not remove the dispersion errors from the flow. From the perspective of the sub-filter scale modelling, this behaviour is correct as the SFS model should only be effective at the smaller scales. Therefore, the dispersion errors must be controlled in a different way. The most accurate and obvious way of achieving this is of course to increase the resolution. However, to remove such effects completely from the boundary layer, the mesh resolution needs to be far higher than is achievable for many practical flows of interest. Therefore for coarser meshes, the dispersion can be controlled by increasing the level of up-winding in the discretisation scheme. This will introduce artificial dissipation but does not appear to delay or prevent the transition from occurring in any of the simulations considered here. From these results, it is recommended that if a very fine mesh cannot be obtained due to the complexity of the geometry or the Reynolds number, then a scheme that minimises the dispersion errors is needed, as these have a significant impact on the boundary layer flow.

### 3.2 Case 2

Using the preceding analysis, Case 2 has been considered using LES with the Dynamic k SFS model and a blended scheme with a 10% level of up-winding. A smaller level of blending has been used here to reduce the dissipation and the presence of dispersion errors will be assessed in the results. Two mesh resolutions are considered, with the parameters shown table 1. Experimental results in [8] show that the acoustic field for this case is dominated by a narrowband component that results from Tollmien-Schlichting waves close to the trailing edge.

The results from both mesh F and mesh G show the growth of a stream-wise instability close to the trailing edge of the foil on both sides. The spectral plots in figure 10 show good agreement

between the two meshes, with both predicting the rapid growth of a narrowband fluctuation towards the trailing edge. Both the upper and lower sides exhibit the same behaviour. The similarity of the amplitude of the fluctuations for the two meshes suggests that the transition region is not contaminated by dispersion errors. These would be identified if the coarser mesh showed larger fluctuations than the finer mesh, particularly upstream of the transition.

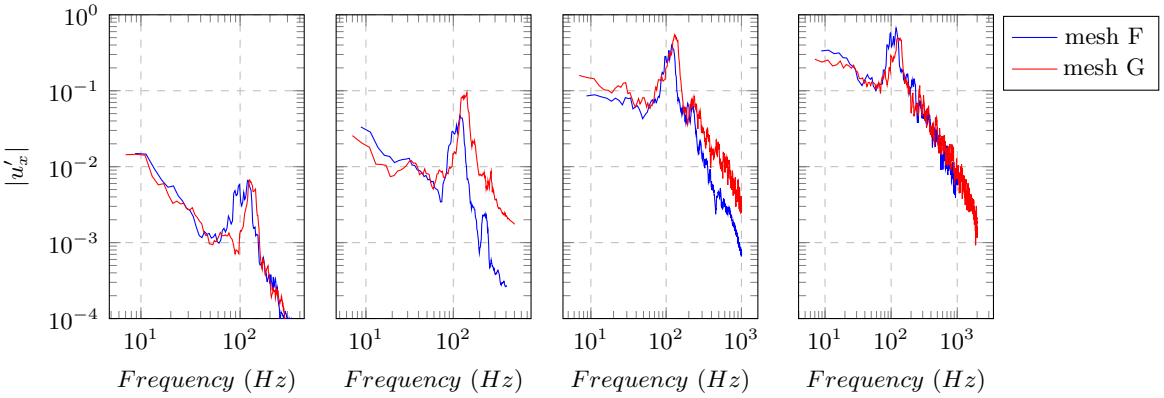


Figure 10: Spectral plots of the streamwise velocity fluctuations in the lower-side boundary layer at $x/c = 0.8,\ 0.9,\ 0.95,\ 1.0$.

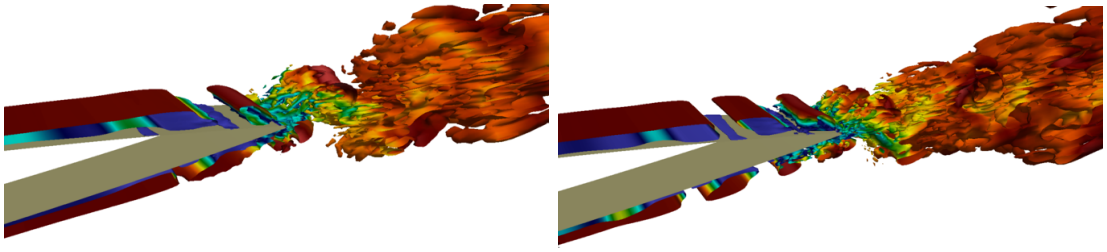

Figure 11: Instantaneous Iso-contours of $Q = 100$ at the trailing edge for Meshes F and G at $t = 20c/U$.

At the trailing edge, the 2D vortical structures on the upper and lower sides interact, creating span-wise fluctuations which lead to fully three-dimensional structures being convected into the near wake of the trailing edge, as shown in figure 11. This behaviour appears to be inconsistent with the experimental analysis in [1], which shows that the amplified T-S waves should produce a mostly 2D near-wake flow field. However, this 2D behaviour was observed for experiments where the foil was at a non-zero angle of attack, with the T-S waves only present at the trailing edge on the pressure side of the foil. For Case 2, we have T-S waves creating large 2D structures on both sides of the foil at the trailing edge, and so it may be that their interaction induces a stronger span-wise instability than is seen in that particular experiment.

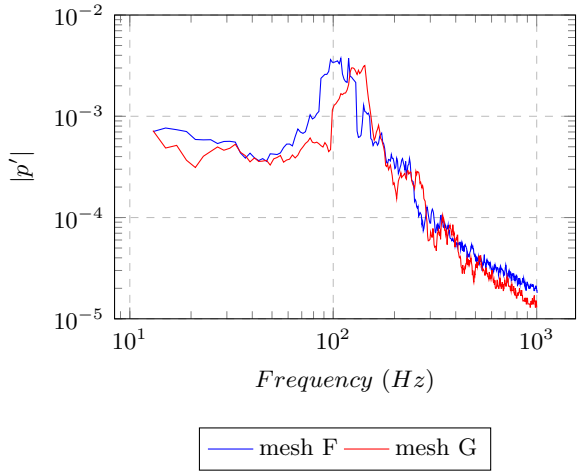


Figure 12: Spectral analysis of the surface pressure fluctuations for Case 2.

The spectral content of the foil surface pressure contains a narrowband component at the same frequency as the instability waves in the boundary layer. This is shown in figure 12 for both meshes. It is noted that mesh G predicts the peak frequency to be 130 Hz whereas mesh F predicts a lower value of 110 Hz. This was also observed for the boundary layer fluctuations.

## 4 CONCLUSIONS

In this study, simulations of the flow over a NACA0012 foil have been conducted using LES and DNS. Two different cases have demonstrated very different behaviours allowing for the relationship between the transition of the boundary layer and the trailing edge flow to be explored. It has been shown that if the boundary layer becomes fully turbulent upstream of the trailing edge, the narrowband fluctuations present during the transitional stage will have disappeared and so will not contribute to the trailing edge noise. If the boundary layer is transitional at the trailing edge, the surface pressure fluctuations will contain tonal components with frequencies equal to those of the instabilities in the boundary layer.

The assessment of the large eddy simulations has identified some important considerations for the sub-filter scale modelling and the discretisation. In order to capture the transition process, the SFS model must remain inactive during the early stages. The constant coefficient Smagorinsky model was shown to be incapable of capturing this process, even for highly resolved meshes and so is not recommended for flows involving transitional boundary layers. Regardless of the modelling approach taken, the importance of grid sensitivity and uncertainty analysis has been highlighted here. By considering how the boundary layer fluctuations change with mesh resolution, dispersion and dissipation errors can be identified. It has been shown that dispersion errors can change the boundary layer dynamics substantially by triggering an earlier transition and so understanding such errors is vital for acoustic analyses. Future work should focus quantifying the contributions of the different error sources and identify a more robust

approach to the discretisation, particularly regarding the use of blending. The impact of the different error sources on the far-field acoustics should also be considered.

**Acknowledgements**

This research was sponsored by the Naval Authority Group at the UK Ministry of Defence and by BMT Group. The Authors also wish to acknowledge the use of the UCL Grace High Performance Computing Facility and associated support services in the completion of this work.

## REFERENCES

[1] Nash, E.C., Lowson, M.V. and McAlpine, A., 1999. Boundary-layer instability noise on aerofoils. Journal of Fluid Mechanics, 382, pp.27-61.

[2] Shan, H., Jiang, L. and Liu, C., 2005. Direct numerical simulation of flow separation around a NACA 0012 airfoil. Computers and Fluids, 34(9), pp.1096-1114.

[3] Jones, L.E., Sandberg, R.D. and Sandham, N.D., 2008. Direct numerical simulations of forced and unforced separation bubbles on an airfoil at incidence. Journal of Fluid Mechanics, 602, pp.175-207.

[4] Solís-Gallego, I., Meana-Fernández, A., Oro, J.F., Díaz, K.A. and Velarde-Suárez, S., 2018. LES-based numerical prediction of the trailing edge noise in a small wind turbine airfoil at different angles of attack. Renewable Energy, 120, pp.241-254.

[5] Wang, J., Zhang, C., Wu, Z., Wharton, J. and Ren, L., 2017. Numerical study on reduction of aerodynamic noise around an airfoil with biomimetic structures. Journal of Sound and Vibration, 394, pp.46-58.

[6] Curle, N., 1955. The influence of solid boundaries upon aerodynamic sound. Proc. R. Soc. Lond. A, 231(1187), pp.505-514.

[7] Williams, J.F. and Hawkings, D.L., 1969. Sound generation by turbulence and surfaces in arbitrary motion. Phil. Trans. R. Soc. Lond. A, 264(1151), pp.321-342

[8] Chong, T.P., Joseph, P.F. and Kingan, M.J., 2013. An investigation of airfoil tonal noise at different Reynolds numbers and angles of attack. Applied Acoustics, 74(1), pp.38-48.

[9] Smagorinsky, J., 1963. General circulation experiments with the primitive equations: I. The basic experiment. Monthly Weather Review, 91(3), pp.99-164

[10] Van Driest, E. R., 1956. On turbulent flow near a wall. Journal of the Aeronautical Sciences, 23(11), pp.1007-1011.

[11] Kim, W.W. and Menon, S., 1999. An unsteady incompressible Navier–Stokes solver for large eddy simulation of turbulent flows. International Journal for Numerical Methods in Fluids, 31(6), pp.983-1017.

[12] Chow, F.K. and Moin, P., 2003. A further study of numerical errors in large-eddy simulations. Journal of Computational Physics, 184(2), pp.366-380.